Supporting Information

One-pot thioetherification of aryl halides with thiourea and benzyl bromide in water catalyzed by Cu-grafted furfural imine functionalized mesoporous SBA-15

John Mondal[a], Arindam Modak[a], Arghya Dutta[a], Sohini Basu[b], S. N. Jha[b], Dibyendu Bhattacharyya[b] and Asim Bhaumik[a]*

[a]*Department of Materials Science, Indian Association for the Cultivation of Science, Jadavpur, Kolkata – 700 032, India*

[b]*Applied Spectroscopy Division, Bhabha Atomic Research Centre, Mumbai-400085, India*

*Address for correspondence. E-mail: msab@iacs.res.in

Table of contents

Section S1: Experimental methods:

Preparation of Cu-grafted mesoporous SBA-15 catalyst. The preparation involves the following sub-steps:

Synthesis of 3-aminopropyl functionalized SBA-15:

Calcined mesoporous silica SBA-15 was synthesized by the reported procedure as described before.[1] 0.1 g calcined SBA-15 was stirred with 0.18 g of 3-aminopropyltriethoxysilane (3-APTES) in $CHCl_3$ at room temperature under N_2 atmosphere for about 12 h. The resulting white solid was filtered, washed with chloroform and dichloromethane and finally dried in air. The white colored solid was designated as (**A**).

Synthesis of imine functionalized mesoporous SBA-15:

A solution of furfural in methanol (5 ml) was added dropwise into the 3-APTES functionalized SBA-15 material (**A**) dispersed into methanol (15 ml) under continuous stirring condition. After the complete addition the reaction mixture was refluxed for about 6 h at 333 K. The color of the reaction mixture was changed into deep yellow and no further color change occurred on further reflux. The reaction mixture was cooled at room temperature and the final

yellow product was collected by filtration, washed repeatedly with hot methanol to remove the unreacted aldehyde. The yellow colored material was dried in air and was designated as (**B**).

Synthesis of Cu(II) anchored mesoporous SBA-15 catalyst:

1 g of respective dried Schiff-base anchored mesoporous SBA-15 (**B)** was suspended in absolute ethanol (20 ml) solution of copper (II) acetate (0.2 g) and was kept under refluxing condition for about 8 h at 363 K. The color of the mesoporous material was slowly changed from deep yellow to light green and no further color change occurred on further reflux. The reaction mixture was cooled at room temperature and the resulting mesoporous material was filtered through suction with thoroughly washing with ethanol. After washing it was dried under vacuum. The light green colored mesoporous material was designated as Cu-grafted mesoporous SBA-15 catalyst (**C**). The outline for the preparation of this Cu(II) anchored SBA-15 catalyst is shown in Scheme 1.

General procedure for Cu(II) grafted mesoporous SBA-15 catalyst mediated one pot thioetherification of aryl halides using thiourea and benzyl bromide in aqueous medium:

To a mixture of K_2CO_3 (552 mg, 4 mmol), thiourea (91 mg, 1.2 mmol) in 5 ml water, aryl halide (1 mmol), benzyl bromide (188 mg, 1.1 mmol) and Cu-grafted catalyst (25 mg) were added and the resulting mixture was heated at 373 K in a oil bath for the appropriate reaction time monitored by TLC (Table 1 & 2). After a period of time the reaction mixture was cooled to room temperature and mixture was extracted with EtOAc. The combined organic layer was washed with water and brine solution. Then the combined organic layer was dried over anhydrous Na_2SO_4 and evaporated to dryness to give the desired aryl alkyl thioethers. The isolated crude product was characterized by ^{1}H and ^{13}C NMR respectively. The one pot

thioetherification reaction of aryl halide by using thiourea and benzyl bromide over catalyst (**C**) in aqueous medium is shown in the scheme 2.

Leaching Test: We have estimated the content of Cu in the fresh catalyst before reaction and that after the reaction using AAS analysis. After the completion of a given reaction the product was filtered off and washed with acetone and then the filtrate was evaporated to dryness. An appropriate amount of nitric acid (30 wt%) was added to the filtrate, and the resulting sample adjusted to 5 wt% nitric acid was applied to characterize the Cu leaching. Cu content in the filtrate was estimated by using a Shimadzu AA-6300 atomic absorption spectrophotometer. Atomic absorption spectrometric analysis of the liquid phase revealed the absence of any detectable Cu in the filtrate solution and that filtrate remains complete colorless. Also ICP-AES analysis was carried out for the reused catalyst. After 6^{th} reaction cycle the Cu content has been marginally decreased to 0.979 mmol g^{-1} (this decrease is within the experimental error of chemical analysis). This result clearly suggests that Cu sites have been covalently grafted with the organic functional groups inside the pore wall, which reduces the leaching of Cu from the catalyst during course of reaction.

Hot filtration test: In order to confirm catalytic activity bound to solid phase hot filtration test was performed. The Cu grafted catalyst (25mg), 4-bromo anisole (1mmol), K_2CO_3 (4 mmol, 552 mg), thiourea (91 mg, 1.2 mmol), benzyl bromide (188 mg, 1.1 mmol) in 5 ml of H_2O was heated to refluxed at 100^oC for 6 h. The Cu-catalyst was filtered off (from the hot reaction mixture) after 6 h. when 50% conversion was achieved (GC and ^1H NMR) and the reaction was continued with the filtrate for another 6 h at the same reaction temperature. Absolutely no increase in the amount of product was observed beyond 50%. It is further noted that copper is

also not detected (AAS) in the liquid phase after the completion of the reaction for 6 h and that the filtrate remains completely colorless.

Three phase test: In order to confirm heterogeneous nature of the catalyst a three phase test was performed. In this experiment a desired amount of amino-functionalized silica (AFS) was refluxed with *p*-bromoacetophenone in dry ethanol in nitrogen atmosphere for 5 h. It was then cooled to room temperature and filtered and repeatedly washed with ethanol to remove unreacted *p*-bromoacetophenone, and dried to obtain the PBA-AFS material. Then a mixture of 4-bromo anisole (1mmol, 187 mg), K_2CO_3 (4 mmol, 552 mg), thiourea (91 mg, 1.2 mmol), benzyl bromide (188 mg, 1.1 mmol) was heated at100^oC for 12 h in presence of Cu-F-SBA-15 catalyst (25 mg). Resulting mixture was then cooled to room temperature, extracted with EtOAc. The combined organic layer was washed with water and brine solution. Then the combined organic layer was dried over anhydrous Na_2SO_4 and evaporated to dryness. The extracted product was analyzed by ^1H NMR which showed the compound was benzyl 4-methoxyphenyl sulfide. The obtained residue was refluxed with 2MHCl and the solution was extracted with Et_2O. The obtained benzyl 4-methoxyphenyl sulfide product makes us sure that 4-bromoacetophenone did not take part in the thioetherification reaction. If any Cu leached to the solution, then anchored *p*-bromoacetophenone would take part in the thioetherification reaction. But this did not occur with Cu-F-SBA-15 catalyst presented here. Thus, this three-phase test provides further evidence that the reaction is truly heterogeneous in nature and there is no leaching of copper during the course of reaction.

Section S2: Characterization Techniques:

Characterization techniques*:* Powder X-ray diffraction patterns are recorded on a Bruker D-8 Advance SWAX diffractometer operated at 40 kV voltages and 40 mA current. The instrument has been calibrated with a standard silicon sample, using Ni-filtered Cu K□ (□ = 0.15406 nm) radiation. Nitrogen adsorption/desorption isotherms are obtained by using a Bel Japan Inc. Belsorp-HP at 77 K. Prior to gas adsorption, samples are degassed for 4 h at 393 K under high vacuum conditions. A JEOL JEM 6700F field emission scanning electron microscope is used for the determination of morphology of the particles. FT IR spectra of the samples are recorded using a Nicolet MAGNA-FT IR 750 Spectrometer Series II. UV-visible diffuse reflectance spectra were recorded on a Shimadzu UV 2401PC with an integrating sphere attachment $BaSO_4$ was used as background standard. High resolution transmittance electron microscopic (HR TEM) images were recorded in a Jeol JEM 2010 transmission electron microscope. Cu loading in the sample was estimated by using a Perkin-Elmer Optima 2100 DV Inductive Coupled Plasma Atomic Emission Spectroscopy (ICP-AES). ^{1}H and ^{13}C NMR experiments were carried out on a Bruker DPX-300 NMR spectrometer. EPR measurements were performed on a Bruker EMX EPR spectrometer at X-band frequency (9.46 GHz) at room temperature (298K). ^{29}Si and ^{13}C solid state magic angle spinning nuclear magnetic resonance (MAS NMR) experiments were carried out to evaluate the different chemical environment of the Si and C atoms in the mesoporous matrix. Bruker advance 500 spectrometer was used here for NMR data recording. The EXAFS measurements of the Cu-F-SBA-15 organometallic samples were carried out in

transmission mode at the dispersive EXAFS beamline (BL-8) at INDUS-2 Synchrotron Source (2.0 GeV, 100 mA).

Section S3: Small angle Powder XRD:

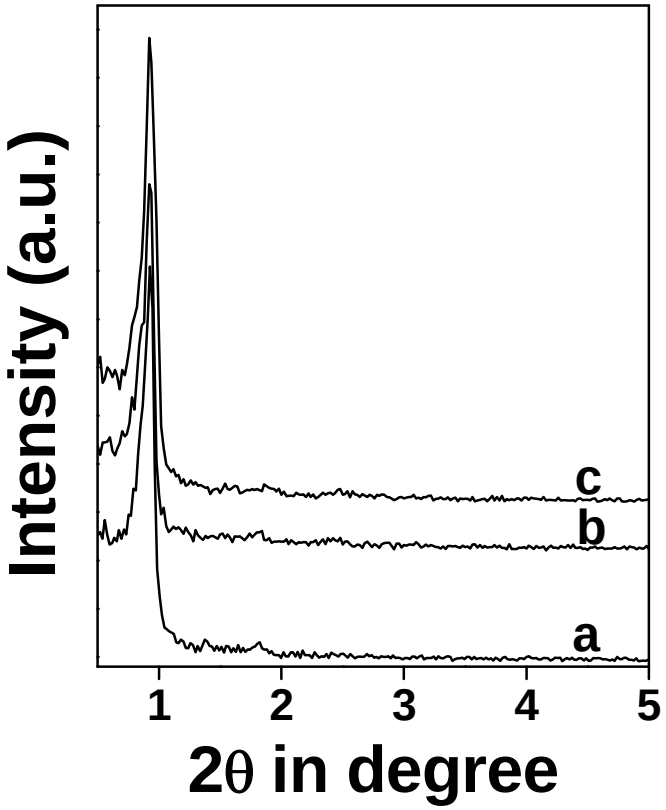

Fig. S1: Small–angle powder XRD pattern of 3-aminopropyl functionalized SBA-15 (a), furfural functionalized (b) and Cu anchored mesoporous SBA-15 (c).

Section S4: Wide angle Powder XRD:

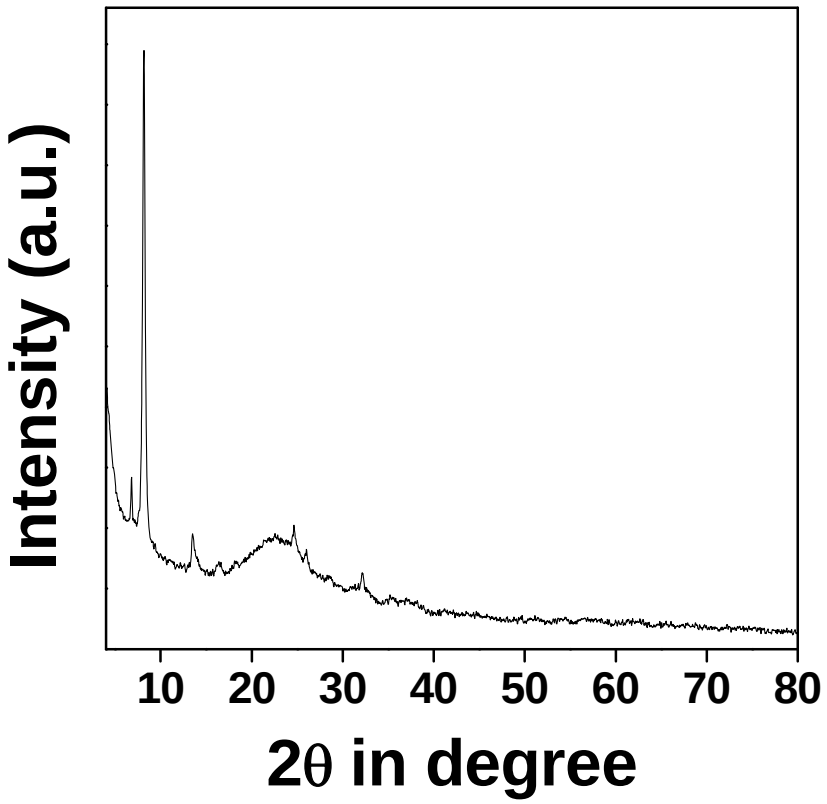

Fig. S2: Wide angle powder XRD pattern of Cu-F-SBA-15.

Wide angle powder X-ray diffraction pattern of Cu-grafted mesoporous material Cu-F-SBA-15 (See supporting information, Figure S2) can be assigned with an orthorhombic phase having unit cell parameters a = 9.722, b = 10.853 and c = 13.197. Unit cell volume has been found to be V = 1392.686 Å^3. *hkl* values for different planes and respective d spacings are given in Table S1. PXRD pattern of the sample has been evaluated with the PXRD pattern calculated by using

Reflex, a software package for crystal determination. The CELSIZ program was used to obtain the lattice parameters along with estimated standard deviations (esd, see supporting information, Table S1).

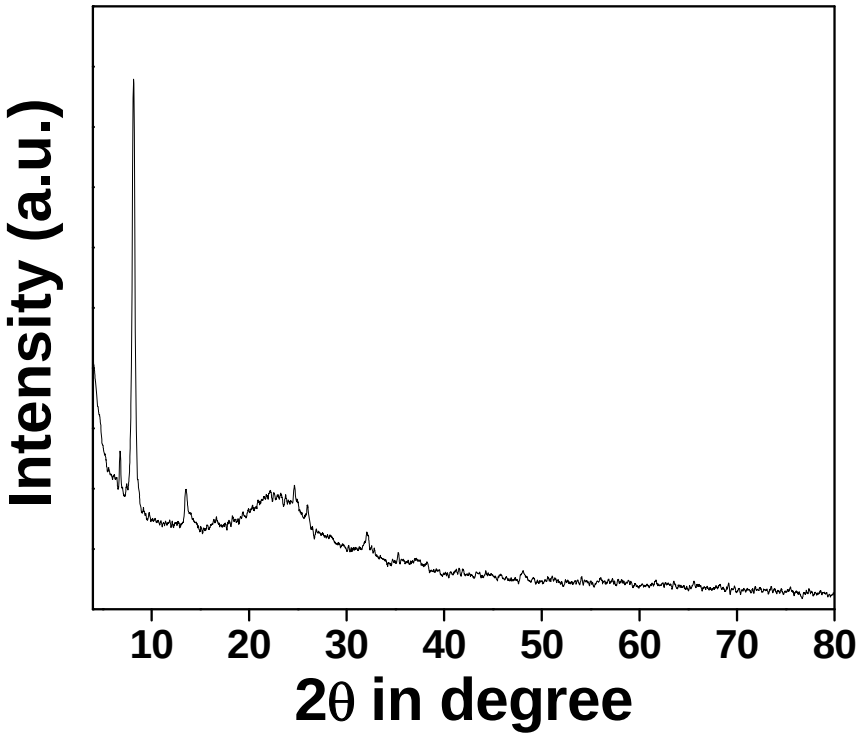

Fig. S3: Wide angle powder XRD pattern of the reused Cu-F-SBA-15 catalyst.

The Cu anchored mesoporous SBA-15 catalyst was characterized after second catalytic cycle by wide angle powder XRD studies. The wide angle powder XRD pattern (Supporting information, Figure S3) suggested that the crystal structure of the mesoporous catalyst has been retained with the characteristic peaks.

Section S5: Nitrogen Sorption Analysis:

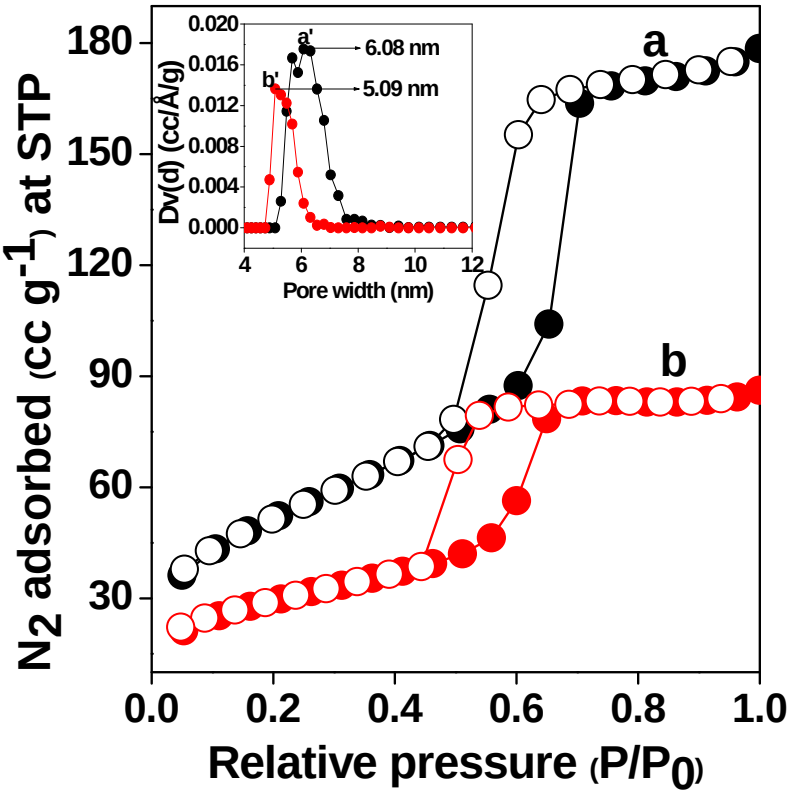

Fig. S4: N_2 adsorption/desorption isotherm of the furfural functionalized mesoporous SBA-15 material (a) and Cu grafted mesoporous SBA-15 catalyst (b). Pore size distributions estimated through NLDFT method is shown in the inset.

N_2 adsorption/desorption isotherms of the furfural functionalized SBA-15 and Cu-anchored mesoporous catalyst Cu-F-SBA-15 at 77 K are shown in the Figure S4 (†ESI). Both the samples show a typical type IV isotherm with a very large hysteresis loop in the 0.5 to 0.8 P/P_o range.[2] The isotherms account for the relatively ordered mesopore and the hysteresis loop, which is the

characteristic for the large tubular pores of SBA-15. The BET surface areas for the furfural functionalized mesoporous SBA-15 (Figure S4a) and Cu-anchored Cu-F-SBA-15 (Figure S4b) are 190 m^2g^{-1} and 117 m^2g^{-1}, respectively and their corresponding pore volumes are 0.263 ccg^{-1} and 0.126 ccg^{-1}, respectively. A considerable decrease in the BET surface area and pore volume upon grafting of Cu at the surface of furfural functionalized SBA-15 material (**B**) clearly suggests that Cu centers have been anchored on the inner surface of the functionalized mesopores. The pore size distributions of the both samples are estimated by employing non-local density functional theory (NLDFT) method shown in the inset of Figure S4 (†ESI). Estimated pore width for furfural functionalized SBA-15 (†ESI: Figure S4a′) is 6.08 nm whereas for Cu-anchored Cu-F-SBA-15 material (†ESI: Figure S4b′) pore size is reduced to 5.08 nm. Calculated pore volume and pore size of the Cu-F-SBA-15 catalyst is adequate to carry out one pot thioetherification of different aryl halides.

Section S6: SEM image of the catalyst:

Fig. S5: SEM image of the Cu-anchored mesoporous SBA-15 catalyst.

FE SEM image of the Cu-grafted SBA-15 catalyst suggests that the material has rod shaped morphology.

Section S7: Infrared Spectroscopy:

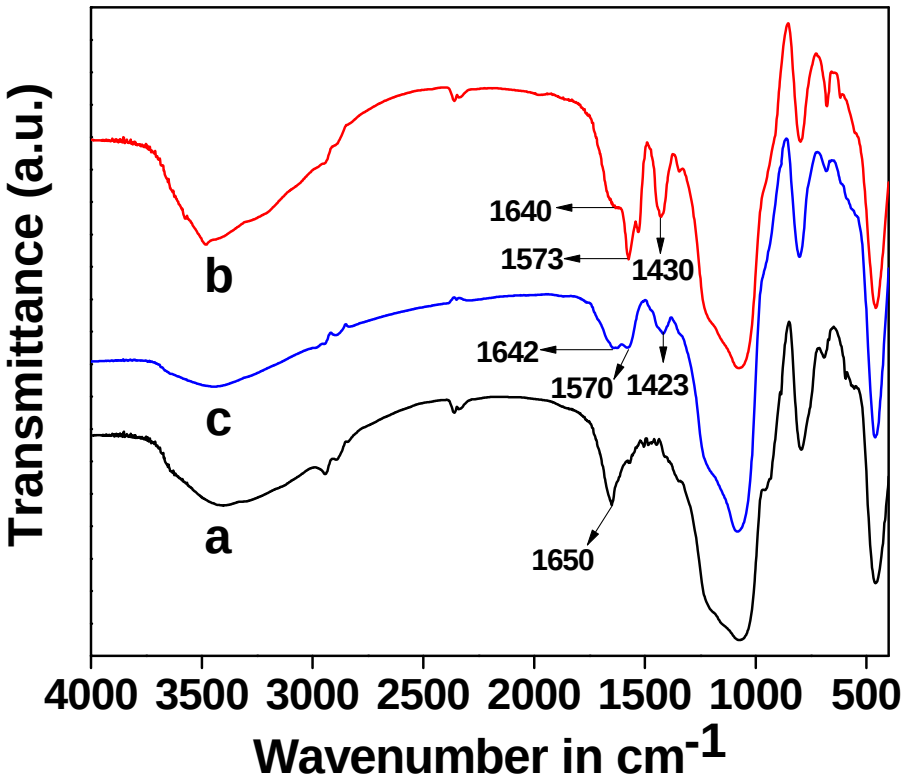

Fig. S6: FT IR spectra of (a) furfural functionalized mesoporous SBA-15, (b) Cu-anchored mesoporous SBA-15 catalyst and (c) Reused Cu-anchored catalyst.

In the IR data for furfural functionalized SBA-15 (See Supporting information, Figure S6a) the peak at 1650 cm^{-1} can be attributed for the C=N bond stretching frequency. For Cu anchored mesoporous SBA-15 material (Supporting information, Figure S6b) the C=N stretching

frequency is shifted to lower wavelength at *ca.*1640 cm^{-1} indicating that C=N bond is coordinated to Copper through the lone pair of electron of nitrogen of Schiff-base ligand. The two strong absorption bands at 1573 cm^{-1} [3] and 1428 cm^{-1} [4] can be assigned to the asymmetric and symmetric vibrations, respectively, of the bridging acetate ions. This result indicates that Cu has been anchored into the mesopores via bridging acetate ligand followed by coordination with N and O donors of furfural functionalized Schiff-base ligand. Moreover, the peaks at 1570 cm^{-1} and 1423 cm^{-1}in the FT IR spectrum (Supporting information, Figure S6c) clearly suggested that acetate bridge structure has been retained in the reused Cu anchored mesoporous SBA-15 catalyst.

Section S8: ***Solid state UV–vis diffuse reflectance Spectroscopy:***

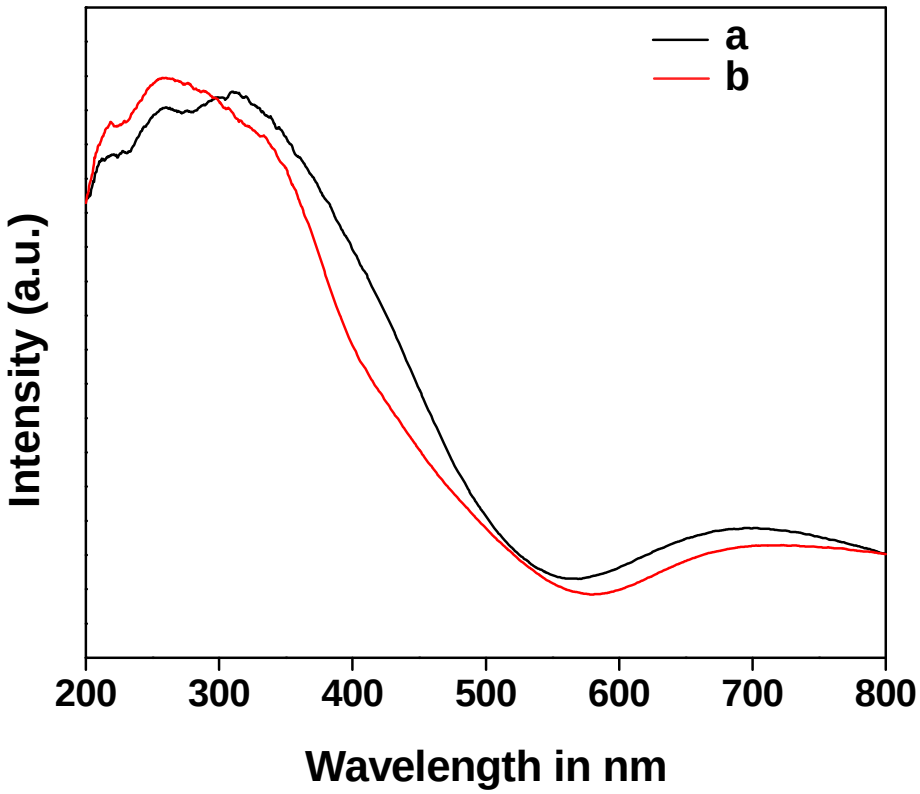

Fig. S7: UV–vis diffuse reflectance spectrum of (a) Cu-anchored mesoporous SBA-15 catalyst and (b) reused catalyst.

In the UV–vis diffuse reflectance spectrum of Cu-anchored mesoporous SBA-15 catalyst (See Supporting information, Figure S7a) a hump at around 300-320 nm is present and a peak that arises around 257 nm can be attributed to the charge transfer band between Cu^{+2} and the oxygen of the ligand. In addition to this, a very broad absorption band in between 600–800 nm is

observed. This could be attributed to the d–d transition of Cu^{+2} ions in a tetragonally distorted octahedral environment,[5] probably arising from the small copper cluster.

Section S9: MAS NMR analysis:

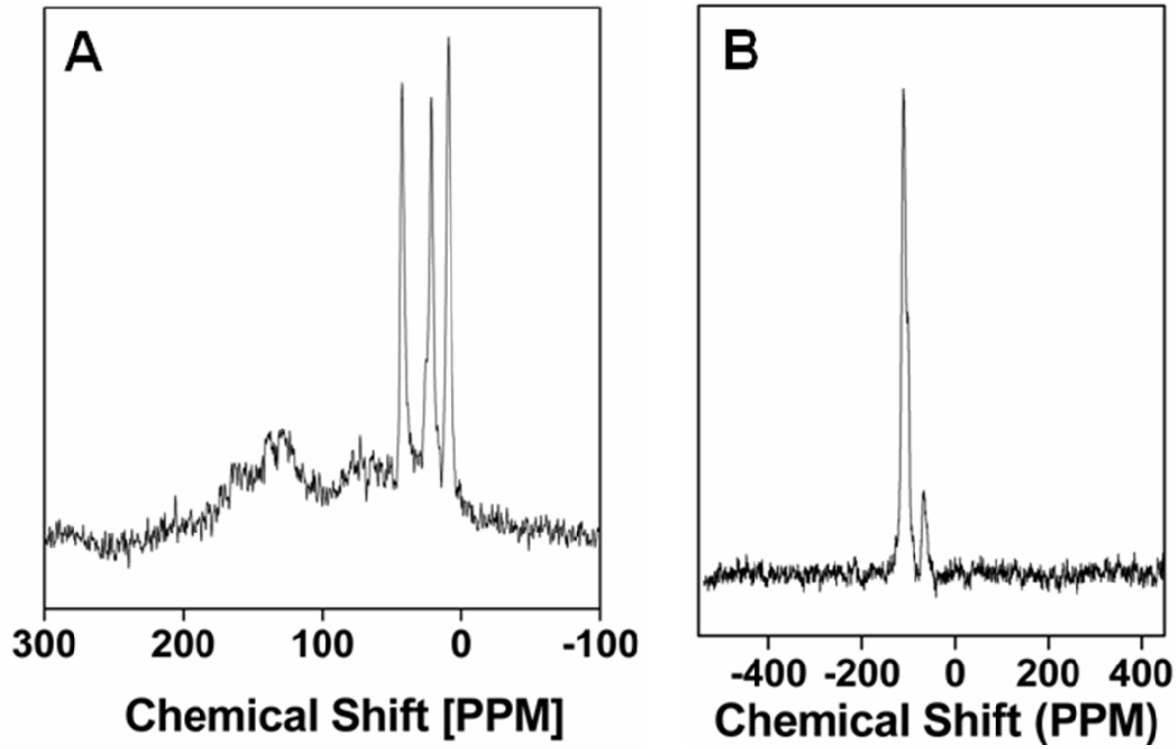

Fig. S8: ^{13}C MAS NMR (A) and 29 Si MAS NMR (B) spectrum of the catalyst

^{13}C and ^{29}Si MAS NMR results provide useful information regarding the chemical environment and the presence of an organic functional group in the hybrid frameworks of the catalyst. The ^{13}C CP MAS NMR spectrum (Figure S8A) for the catalyst exhibits three strong signals at 9.1, 21.8 and 43.5 ppm which can be assigned to the aliphatic propyl group attached with Si of the hybrid framework. Broad signals with maximums at 62.8, 128.8, 137.6 are attributed to imine-C, carbon atoms of the furfural ring, respectively. On the other hand the ^{29}Si MAS NMR spectra of the catalyst (Figure S8B) shows two broad signals with the chemical shifts at –67.1and –111.7 ppm, which could be attributed to the T^3 ($(OH)(OSi)_3Si–R$) and Q^4 ($Si(OSi)_4$)

species, respectively. These MAS NMR experimental results indicate that the functional group bearing the organic moiety is covalently grafted inside the pore walls of the mesoporous catalyst. The strong signals of ^{13}C CP-MAS NMR further confirm that high loadings of organic groups on the solid surface of the mesoporous catalyst.

Section S10: EPR studies:

Copper acetate monohydrate exists as dimer at room temperature. As a result EPR spectrum will be obtained at the "half field" suggesting dimeric Cu species with the $g_{\perp}$ and $g_{\parallel}$ are 2.08 and 2.38 respectively. The broad spectrum obtained for Cu-acetate which is due to the interdimer magnetic separation. But EPR spectrum of our Cu-F-SBA-15 material excludes the presence of any significant antiferromagnetic exchange between the two Cu centers. Because in our catalyst Cu is in distorted square planar symmetry surrounded by the organic furfural imine ligands with the Cu-Cu distance 3.37 Å. This Cu-Cu distance is larger than the normal Cu-Cu distance (2.64 Å) in copper acetate. The acetate bridge ligands (obtained from IR spectra) axially coordinate the Cu atom leading to appreciable distortions. As a result with the increase of distance from metal center to metal center exchange coupling reduces. It has been suggested that the distance is too long to transmit any significant interaction. That is why in Cu-F-SBA-15 material we obtained hyperfine splitting pattern.[10]

In a planar bonding $g_{\parallel}$ decreases and $A_{\parallel}$ increases in the order of CuO_4>CuO_3N>CuO_2N_2>CuN_4. Here in our EPR spectrum for Cu-F-SBA-15 catalyst $g_{\parallel}$ and $A_{\parallel}$ are 2.26 and 172G respectively. The type of coordination units are confirmed from the observed $A_{\parallel}$ and $g_{\parallel}$ values. Thus, from our EPR results we can confirm that $CuON_3$ discrete units are present.[11]

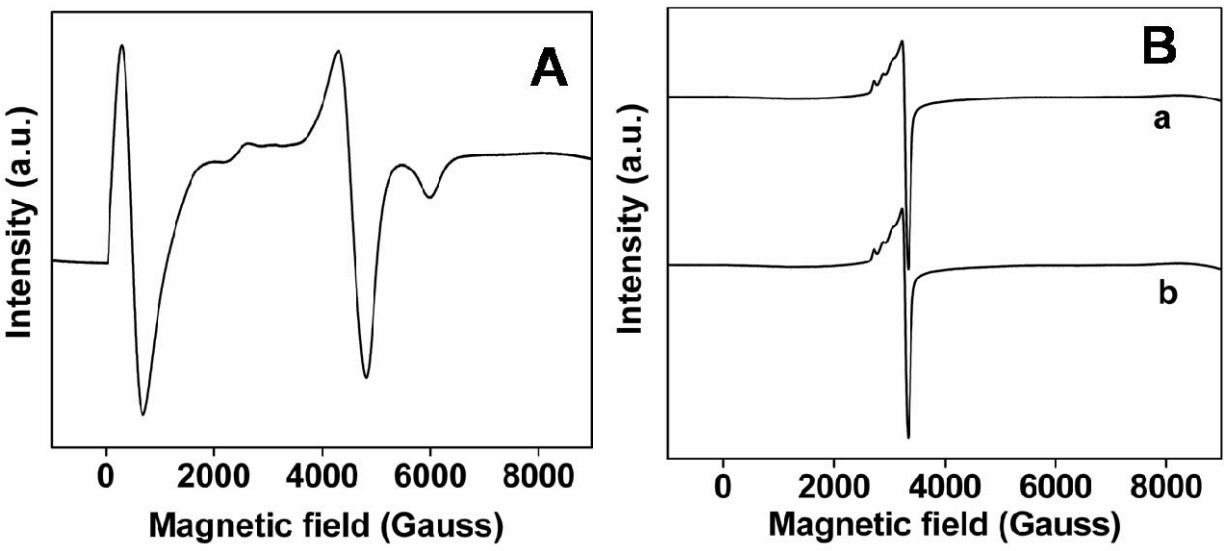

Fig. S9: EPR spectra of $Cu(OAc)_2.H_2O$ (A) and Cu-F-SBA-15 catalysts (B): fresh (a) and reused (b).

Section S11: EXAFS data:

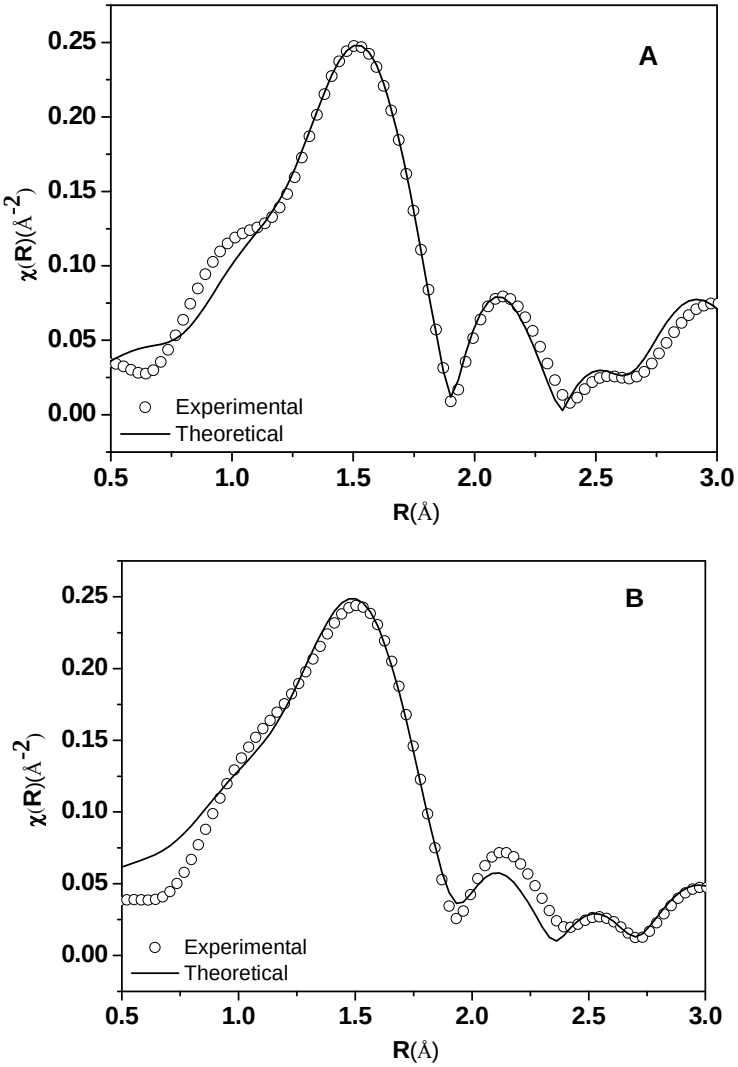

Fig. S10: Radial distribution function ($\chi(R)$ versus R) around Cu atom (without phase-shift correction) for the samples Cu anchored catalyst (A) and reused catalyst (B) as obtained from the experimental $\mu(E)$ versus E spectra

To get a more quantitative insight, the experimentally obtained $\chi(R)$ versus R spectra of the Cu-F-SBA-15 samples have been fitted with theoretically generated spectra. To start with, the

experimental spectrum the known crystallographic structure of CuO has been used to generate the theoretical $\chi(R)$ versus R spectrum of the sample. A Cu-O first shell at a distance of 1.95 Å and having a coordination number of 4, a second Cu-O shell at a distance of 2.78 Å and having a coordination number of 2 and a third Cu-Cu shell at distance of 2.90 Å and having coordination of 4 have been used to generate the theoretical spectrum of the sample upto a distance of 4 Å from the central Cu atom.[6-8] Subsequently, the theoretically generated $\chi(R)$ versus R spectrum has been fitted with the experimentally obtained spectrum with the bond distance (R), coordination number (N) and the Debye-Waller factor (σ^2, representing the thermal and structural disorders) as fitting parameters. The experimentally obtained $\chi(R)$ versus R spectra of the catalyst (A) and reused catalyst (B) were subsequently been fitted the best-fit curves in Fig. S9 and the best fit parameters have been given in Table S2. On the basis of the Scheme 1, four oxygen atoms form the acetate and furfural ligands present in the Cu grafted catalyst. The oxygen co-ordinations in the 1st Cu-O shell and the Cu-Cu bond lengths or the radii of the 3rd shell of the Cu catalyst and the reused catalyst remain same. This results clearly proves that catalyst environment and the co-ordination number around the Cu atom of the reused catalyst remains unaltered during the course of the catalytic reaction. The EXAFS value for the Cu-F-SBA-15 catalyst was compared with the literature EXAFS value of solid copper acetate where the coordination of oxygen with copper was observed. The Cu-O1 agrees well with the catalyst which is 1.97 Å. But Cu-Cu distance is greater than the copper acetate. The Cu-Cu distance in copper acetate is 2.64 Å.[9] But in the catalyst Cu-Cu bond has been elongated to 3.37 Å. The organic furfural imine ligand helps the distortion as a result Cu bond distance increases and catalyst assumes distorted square planar geometry.

Thus, EPR and EXAFS result clearly indicated that our Cu-F-SBA-15 material is not simply SBA-15 impregnated with copper acetate or Cu-nanocluster at the surface of mesoporous silica, rather Cu is bound to furfural imine at the surface of mesoporous silica as shown in Scheme 1.

Section S12: ^{1}H and ^{13}C nmr data:

^{1}H and ^{13}C NMR chemical shifts for different coupling products reported in Table 1.

Benzyl phenyl sulfide (Table 1, entry 1): ^{1}H NMR (300 MHz, $CDCl_3$) δ 7.74-7.71 (1H, d, J=9 Hz), 7.39-7.14 (7H, m), 7.25 (2H, t), 3.69 (2H, s); ^{13}C NMR (300 MHz, $CDCl_3$) δ 138.1, 137.3, 130.2, 129.4, 128.6, 128.4, 127.4, 126.9, 43.2.

Benzyl 4-nitrophenyl sulfide (Table 1, entry 2): ^{1}H NMR (300 MHz, $CDCl_3$) δ 7.91-7.84 (4H, m), 7.30-7.18 (5H, m), 3.56 (2H, s); ^{13}C NMR (300 MHz, $CDCl_3$) δ 147.8, 138.7, 137.4, 129.5, 128.5, 127.5, 127.0, 124.9, 35.6.

Benzyl 4-methoxyphenyl sulfide (Table 1, entry 3): ^{1}H NMR (300 MHz, $CDCl_3$) δ 7.52-7.49 (2H, d, J=9 Hz), 7.28-7.20 (5H, m), 6.64-6.61 (2H, d, J=9 Hz), 3.70 (3H, s), 3.56 (2H, s); ^{13}C NMR (300 MHz, $CDCl_3$) δ 159.3, 138.1, 129.3, 128.9, 128.7, 127.3, 126.9, 116.3, 55.2, 35.5.

Benzyl 4-methylphenyl sulfide (Table 1, entry 4): ^{1}H NMR (300 MHz, $CDCl_3$) δ 7.50-7.47 (2H, d, J=9 Hz), 7.28-7.19 (5H, m), 6.85-6.82 (2H, d, J=9 Hz), 3.53 (2H, s), 2.21 (3H, s); ^{13}C NMR (300 MHz, $CDCl_3$) δ 138.0, 137.1, 131.1, 129.3, 128.9, 128.3, 127.3, 126.8, 35.5, 20.9.

Benzyl 4-formylphenyl sulfide (Table 1, entry 5): ^{1}H NMR (300 MHz, $CDCl_3$) δ 9.82 (1H, s), 7.61-7.52 (3H, q), 7.21-7.09 (6H, m), 3.47 (2H, s); ^{13}C NMR (300 MHz, $CDCl_3$) δ 190.9, 138.0, 137.3, 135.0, 130.9, 129.3, 128.9, 128.5, 126.9, 35.6.

Benzyl 4-acetylphenyl sulfide (Table 1, entry 6): ^{1}H NMR (300 MHz, $CDCl_3$) δ 7.76-7.73 (2H, d, J=9 Hz), 7.54-7.51 (2H, d, J=9 Hz), 7.30-7.19 (5H, m), 3.56 (2H, s), 2.50 93H, s); ^{13}C NMR (300 MHz, $CDCl_3$) δ 196.8, 137.9, 137.2, 132.0, 129.8, 128.8, 127.2, 126.8, 35.5, 29.5.

Benzyl 4-cyanophenyl sulfide (Table 1, entry 7): ^{1}H NMR (300 MHz, $CDCl_3$) δ 7.58-7.56 (2H, d, J=6 Hz), 7.44-7.42 (2H, d, J=6 Hz), 7.26-7.16 (5H, m), 3.52 (2H, s); ^{13}C NMR (300 MHz, $CDCl_3$) δ 138.2, 137.4, 133.5, 129.5, 129.0, 128.5, 128.1, 127.0, 118.1, 111.3, 35.7.

Benzyl 4-hydroxy-3-formyl phenyl sulfide (Table 1, entry 8): ^{1}H NMR (300 MHz, DMSO-d_6) δ 10.2 (1H, s), 7.70 (1H, s), 7.63-7.60 (1H, d, J=9 Hz), 7.39-6.98 (6H, m), 6.98-6.95 (1H, d, J=9 Hz), 3.63 (2H, s); ^{13}C NMR (300 MHz, DMSO-d_6) δ 189.6, 160.2, 138.4, 130.4, 129.3, 128.8, 128.3, 127.2, 126.8, 124.0, 110.4, 35.1.

Benzyl pyrazoyl sulfide (Table 1, entry 9): ^{1}H NMR (300 MHz, $CDCl_3$) δ 7.54 (2H, s), 7.36-7.22 (5H, m), 3.59 (2H, s); ^{13}C NMR (300 MHz, $CDCl_3$) δ 138.0, 134.2, 129.2, 127.7, 126.8, 35.5.

3-thiobenzyl Benzyl alcohol (Table 1, entry 13): ^{1}H NMR (300 MHz, $CDCl_3$) δ 7.20-7.01 (9H, m), 4.46 (2H, s), 3.46 (2H, s); ^{13}C NMR (300 MHz, $CDCl_3$) δ 143.2, 138.0, 134.1, 129.5, 128.5, 128.3, 127.4, 126.8, 126.7, 124.7, 63.8, 35.5.

Benzyl 4-aminophenyl sulfide (Table 1, entry 15): ^{1}H NMR (300 MHz, $CDCl_3$) δ 7.20-7.06 (5H, m), 6.96-6.92 (2H, m), 6.43-6.36 (2H, t), 4.47 (2H, s), 3.45 (2H, s); ^{13}C NMR (300 MHz, $CDCl_3$) δ 145.2, 138.0, 129.3, 128.9, 127.5, 126.4, 122.7, 116.0, 43.1.

Section S13: Recyclability test:

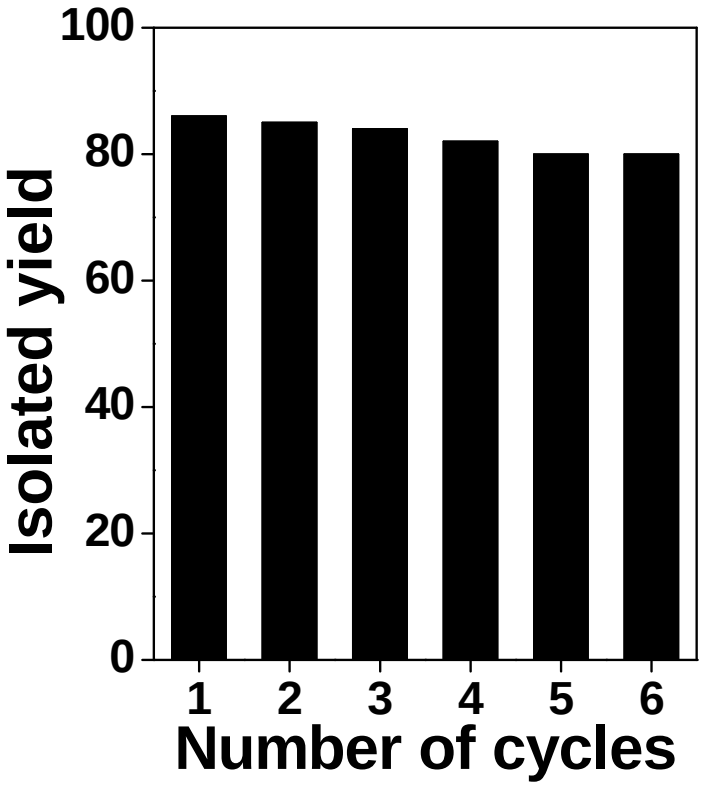

Fig. S11: Recycling efficiency Cu-anchored mesoporous SBA-15 catalyst.

Section S14

Table S1. Unit cell parameters of Cu-F-SBA-15 material**.**

Phase: Orthorhombic				
Parameters		Deviations		
a = 9.722		0.0297		
b = 10.853		0.0282		
c = 13.197		0.0442		
V = 1392.686		ESD 7.29		
h	k	l	2θ [degree]	d [Å]
0	0	1	6.79	13.018
0	1	0	8.13	10.875
0	0	2	13.51	6.554
0	3	0	24.64	3.613
0	2	3	26.01	3.425
3	2	0	32.17	2.782

Table S2. Best-fit parameters of the bond distance, coordination number and the Debye-Waller factors for the catalyst samples.

		Catalyst	Reused Catalyst
Cu-O1	R (Å)	1.97	1.95
	N	2.5	2.44
	σ^2	0.005	0.006
Cu-O2	R(Å)	2.71	2.62
	N	0.9	0.9
	σ^2	0.005	0.003
Cu-Cu	R(Å)	3.37	3.5
	N	1.5	0.9
	σ^2	0.005	0.005

Table S3. Screening of different catalysts for thioetherification reaction

Entry	Catalyst	Time (h)	Yield(%)
1	No catalyst	15	0.0
2	SBA-15	15	0.0
3	Furfural-SBA-15	15	0.0
4	$Cu(OAc)_2.H_2O$	15	42.0
5	Cu nanoparticles supported over SBA-15	15	45.0

Section S15:

References

1	J.-Q. Wang, L. Huang, M. Xue, Y. Wang, L. Gao, J. H. Zhu, and Z. Zou, *J. Phys. Chem. C*, 2008, **112**, 5014-5022.
2	D. Y. Zhao, Q. S. Huo, J. L. Feng, B. F. Chmelka and G. D. Stucky, *J. Am. Chem. Soc*., 1998, **120**, 6024–6036.
3	A. Roth, J. Becher, C. Herrmann, H. Go1rls, G. Vaughan, M. Reiher, D. Klemm and W. Plass, *Inorg. Chem.*, 2006, **45**, 10066-10076.
4	W. Chen, J. Y. Wang, C. Chen, Qi Yue, H. M. Yuan, J. S. Chen and S. N. Wang, *Inorg. Chem.*, 2003, **42**, 944-946.
5	G. Zhang, J. Long, X. Wang, Z. Zhang, W. Dai, P. Liu, Z. Li, L. Wu and X. Fu, *Langmuir*, 2010, **26**, 1362-1371.
6	D. Bhattacharyya, A. K. Poswal, S. N. Jha, and S. C. Sabharwal, *Nucl. Inst. Method Phys. Res. A* 2009, **609**, 286.
7	S. Basu, B. S. Naidu, M. Pandey, V. Sudarsan, S. N. Jha, D. Bhattacharyya, R. K.Vatsa and R. J. Kshirsagar, *Chem. Phys. Lett*., 2012, **25**, 528.
8	S. Basu, S. Varma, A. N. Shirsat, B. N. Wani, S. R. Bharadwaj, A. Chakrabarti, S. N. Jha and D. Bhattacharyya, *J. Appl. Phys*., 2012, **111**, 053532.
9	D. Galland, M. Belakhovsky, F. Medrignnac and M. Pineri, *Polymer*, 1986, **27**, 883-888.

10	(a) P. Harrock and M. Melni, *Can. J. Chem.*, 1985, **63,** 52-56; (b) P. A. Chetcuti, A. Liegard, G. Rihs, G. Rist and A. Schweiger, *Helv. Chim. Acta*, 1991, **74**, 1591-1599; (c) T. Dziembowska, N. Guskos, J. Typek, R. Szymczak, V. Likodimos, S. Glenis, C.L. Lin, M. Wabia, E. Jagodzinska, and E. Fabrycy, *Mater. Res. Bull.,* 1999, **34**, 943–954; (d) M. R. Mendoza-Quijano, G. Ferrer-Sueta, M. Flores-Álamo, N. Aliaga-Alcalde, V. Gómez-Vidales, V. M. Ugalde-Saldívara and Laura Gasque*, Dalton Trans.*, 2012, **41**, 4985–4997; (e) C. D. Syme, R. C. Nadal, S. E. J. Rigby, and J. H. Viles , *J. Biol. Chem.*, 2004, **279**, 18169-18177; (f) G. M. Zats, H. Arora, R. Lavi, D. Yufit and L. Benisvy, *Dalton Trans.*, 2012, **41**, 47-49.
11	M. Naderi, J. L. Pickett, M. J. Chinn and D. R. Brown, *J. Mater. Chem*., 2002, **12**, 1086–1089.